The microtubule-associated protein DCAMKL1 regulates osteoblast function via repression of Runx2

The microtubule-associated protein DCAMKL1 regulates osteoblast function via repression of Runx2

Weiguo Zou,[1] Matthew B. Greenblatt,[2] Nicholas Brady,[3] Sutada Lotinun,[4] Bo Zhai,[5] Heather de Rivera,[3] Anju Singh,[6] Jun Sun,[1] Steven P. Gygi,[5] Roland Baron,[4] Laurie H. Glimcher,[3] and Dallas C. Jones[7]

[1]State Key Laboratory of Cell Biology, Institute of Biochemistry and Cell Biology, Shanghai Institutes for Biological Sciences, Chinese Academy of Sciences, Shanghai 200031, China
[2]Department of Pathology, Brigham and Women's Hospital, Boston, MA 02115
[3]Department of Medicine, Weill Cornell Medical College, New York, NY 10065
[4]Department of Oral Medicine, Infection, and Immunity, Harvard School of Dental Medicine; and [5]Department of Cell Biology, Harvard Medical School; Harvard University, Boston, MA 02115
[6]National Center for Advancing Translational Sciences, National Institutes of Health, Bethesda, MD 20892
[7]Merck Research Laboratories, Boston, MA 02115

Osteoblasts are responsible for the formation and mineralization of the skeleton. To identify novel regulators of osteoblast differentiation, we conducted an unbiased forward genetic screen using a lentiviral-based shRNA library. This functional genomics analysis led to the identification of the microtubule-associated protein DCAMKL1 (Doublecortin-like and CAM kinase–like 1) as a novel regulator of osteogenesis. Mice with a targeted disruption of Dcamkl1 displayed elevated bone mass secondary to increased bone formation by osteoblasts. Molecular experiments demonstrated that DCAMKL1 represses osteoblast activation by antagonizing Runx2, the master transcription factor in osteoblasts. Key elements of the cleidocranial dysplasia phenotype observed in *Runx2*$^{+/-}$ mice are reversed by the introduction of a *Dcamkl1*-null allele. Our results establish a genetic linkage between these two proteins in vivo and demonstrate that DCAMKL1 is a physiologically relevant regulator of anabolic bone formation.

CORRESPONDENCE
Weiguo Zou:
zouwg94@sibcb.ac.cn

Abbreviations used: 3-D, three-dimensional; Alp, alkaline phosphatase; API, Alp index; MSC, mesenchymal stem cell; TRAP, tartrate-resistant acid phosphatase.

Osteoblasts are specialized cells of mesenchymal origin that synthesize the extracellular matrix proteins required for mineralization of the embryonic skeleton (Erlebacher et al., 1995; Karsenty and Wagner, 2002). The high synthetic capacity of the osteoblast is also essential for maintaining bone mass during postnatal remodeling (Harada and Rodan, 2003). As bone accrues damage as the result of physiological exposure to mechanical stress, multinucleated giant cells termed osteoclasts localize at these sites and resorb the existing bone through an acidic and enzymatic process (Boyle et al., 2003). Osteoblasts are then recruited to sites of resorption where they secrete both collagenous and noncollagenous proteins that form the extracellular matrix that will give rise to newly mineralized bone (Martin et al., 2009). Functional dysregulation of osteoblasts during this remodeling process can affect bone density and contributes to the pathogenesis of skeletal disorders, such as osteoporosis, the most common skeletal disease worldwide (Zaidi, 2007). Thus, numerous regulatory pathways that control osteoblast differentiation and function exist to ensure that skeletal formation and remodeling proceed unperturbed.

Several regulatory mechanisms influencing osteoblast differentiation center on controlling the activity of the transcription factor Runx2 (Lian et al., 2006). The expression of Runx2 in mesenchymal precursors is essential for their commitment to the osteoblast lineage as demonstrated by the lack of both mature osteoblasts and a mineralized skeleton in *Runx2*$^{-/-}$ mice (Komori et al., 1997; Mundlos et al., 1997; Otto et al., 1997). Although the presence of a single copy of *Runx2* is sufficient for mineralization to occur

The Rockefeller University Press $30.00
J. Exp. Med. 2013 Vol. 210 No. 9 1793-1806
www.jem.org/cgi/doi/10.1084/jem.20111790

The Journal of Experimental Medicine

in vivo, *Runx2*$^{+/-}$ mice still exhibit delayed closure of the fontanelles and clavicular hypoplasia (Otto et al., 1997). The skeletal phenotype of *Runx2*$^{+/-}$ mice resembles the cleidocranial dysplasia phenotype arising from *Runx2* haploinsufficiency in humans (Mundlos et al., 1997). The presence of these skeletal pathologies in both humans and mice underscores the importance of precise regulation of Runx2 levels and activity during osteogenesis.

Although a significant number of molecules, like Runx2, have been described to regulate osteoblast biology, the complex temporal signaling networks that govern this process suggest that many regulators of osteogenesis remain to be identified. Historically, molecules critical for osteoblast differentiation and function have been identified through single gene mutations in humans and mice. Although this approach results in the identification of genes that are biologically relevant to the skeletal system, it is limited by the rate at which new genes are identified. Using a high-throughput forward genetic approach could accelerate the identification of additional molecules and signaling pathways that regulate osteoblast biology. Unbiased functional genomics approaches using RNAi-based loss-of-function screens have been successful in identifying key molecules that regulate several physiological and pathological processes (Moffat et al., 2006; Vasudevan et al., 2009; Kim et al., 2010). We therefore used arrayed libraries of lentiviral-based shRNAs to assess individual gene function during osteoblast differentiation in vitro.

DCAMKL1 (Doublecortin-like and CAM kinase–like 1) is a serine-threonine kinase of the CAMK family, showing homology to Doublecortin (DCX), which is mutated in X-linked lissencephaly (Omori et al., 1998; Burgess et al., 1999; Matsumoto et al., 1999; Sossey-Alaoui and Srivastava, 1999). An evolutionarily conserved Doublecortin (DC) domain that is able to bind to tubulin and enhance microtubule polymerization exists in the N terminus of DCAMKL1 and DCX. Both DCAMKL1 and DCX are highly expressed in the developing brain and may function together to regulate microtubules involved in neuronal migration. Dcamkl1-deficient mice are viable and fertile and display modest neural abnormalities (Deuel et al., 2006; Koizumi et al., 2006), suggesting that Doublecortin may provide partial functional compensation. Subsequent studies have demonstrated that DCAMKL1 exhibits variable expression patterns in embryonic and adult tissues outside of the central nervous system, suggesting that this protein may control additional physiological processes (May et al., 2008; Gerbe et al., 2009; Itzkovitz et al., 2012).

In this study, we describe a previously unknown role for DCAMKL1 within the skeletal system to regulate osteoblast functions and bone formation. We identified DCAMKL1 through a functional genomics approach that used RNAi-based loss-of-function screens to assess individual gene function during osteoblast differentiation in vitro. Mice lacking Dcamkl1 exhibit an increase in osteoblast numbers, elevated bone mass, and increased rates of bone formation, which confirm that DCAMKL1 is a negative regulator of anabolic bone formation. This occurs via the ability of DCAMKL1 to control osteoblast differentiation through antagonism of Runx2 transcriptional activity. Analysis of *Dcamkl1/Runx2* compound mutant mice revealed partial rescue of the clavicular hypoplasia, runting, and calvarial hypomineralization seen in *Runx2* haploinsufficiency. These results provide genetic evidence that DCAMKL1 is an important novel regulator of Runx2, the master transcription factor for the osteoblast lineage.

RESULTS

A functional genomics approach to identify novel regulators of osteoblast differentiation

To identify unique genes that dictate the differentiation of mesenchymal stem cells (MSCs) into the osteoblast lineage, we initiated an unbiased screen that used a lentiviral-based shRNA library that targeted ~1,500 different human kinases, phosphatases, and receptors with each gene in the library being covered by four to five separate shRNAs (http://www.broadinstitute.org/rnai/trc/lib; Moffat et al., 2006). This screen was conducted in primary human MSCs that under the appropriate culture conditions can be reproducibly differentiated along the osteoblast lineage. As the human MSCs differentiate into osteoblasts, they up-regulate expression of the characteristic osteoblast marker alkaline phosphatase (Alp), which can be quantified via a simple colorimetric assay (Fig. 1 A). We used this characteristic of hMSCs to analyze the capability of the various shRNAs to alter differentiation into the osteoblast lineage. As proof of principle that hMSC lineage commitment can be altered, we demonstrated that transduction of these cells with *Runx2*-specific shRNAs resulted in reduced osteogenesis, as shown by staining with Fast blue (Fig. 1 B). For the large-scale screen, Alp levels of lentivirus-infected MSCs were quantified after a 7-d culture period and were normalized to cell number with Alamar blue (Fig. 1 C). An Alp index (API) is assigned to each shRNA sample, and a list of candidates were identified in the screen based on the API of known genes that regulate MSC differentiation (see Materials and methods). Our screen and subsequent analysis demonstrated robust induction of Alp levels by shRNA directed against *Dcamkl1*, a member of the doublecortin family of microtubule-associated proteins (Omori et al., 1998; Burgess et al., 1999; Matsumoto et al., 1999; Sossey-Alaoui and Srivastava, 1999). We next asked whether reduction of DCAMKL1 protein levels by individual shRNAs correlated with osteoblast phenotype. As shown in Fig. 1 D, those hairpins that augmented Alp levels also reduced DCAMKL1 protein levels, as measured by Western blot analysis. More importantly, Dcamkl1-targeted shRNAs also induced elevated levels of mineral deposition as determined by von Kossa staining (Fig. 1 E). Collectively, these data demonstrate that knockdown of Dcamkl1 by shRNA hairpins can augment the differentiation of osteoblasts from undifferentiated human mesenchymal precursors in vitro.

DCAMKL1 regulates mouse osteoblast differentiation in vitro

To further explore the function of DCAMKL1 in osteoblastogenesis, we sought to establish whether this protein functions in the mouse skeletal system. In situ hybridization of

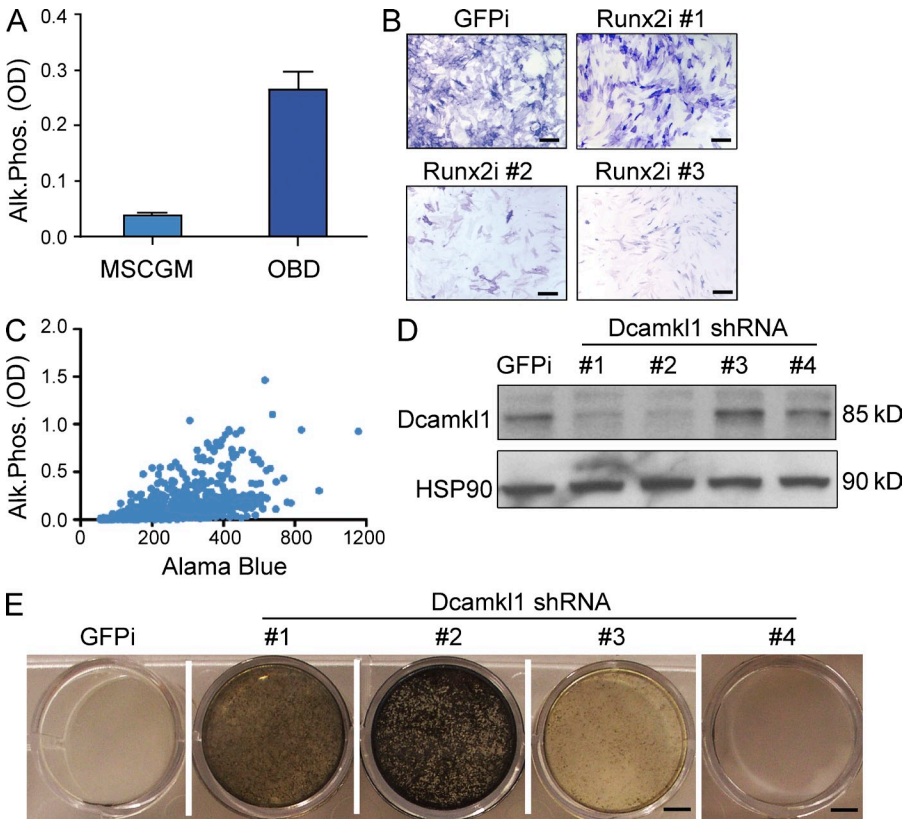

Figure 1. Identification of DCAMKL1 in a lentiviral-based shRNA screen in hMSCs. (A) Alp in MSCs cultured in basal maintenance media (MSCGM) or in osteoblast differentiation media (OBD). Results are presented as the mean ± SD of triplicates of cells cultured in 96-well plates and are representative of two independent experiments. (B) Fast blue staining for Alp-positive cells after infection with lentivirus expressing Runx2-specific shRNAs 1–3. The data are representative of two independent experiments. (C) XY scatter plot of Alp (y axis) and cell number (x axis) depicting the effects of individual shRNA on hMSC differentiation. (D) Analysis of DCAMKL1 protein expression in hMSCs after infection with control shRNA targeting GFP or Dcamkl1-specific shRNAs. (E) von Kossa staining of hMSCs infected with lentivirus expressing control or *Dcamkl1* shRNAs cultured in osteoblast differentiation media for 21 d. The data are representative of two independent experiments. Bars: (B) 20 µm; (E) 4 mm.

embryonic day (E) 16.5 embryos revealed expression of *Dcamkl1* at several locations throughout the developing skeleton, including the vertebrae, ribs, and limbs (Fig. 2 A). We further explored whether *Dcamkl1* was expressed in primary osteoblasts harvested from the calvarium of neonatal mice and compared its expression in osteoblasts with that in other cellular populations within the skeleton. As shown in Fig. 2 B, *Dcamkl1* mRNA can be detected in whole bone, primary osteoblasts and to a much lesser extent in primary osteoclasts. Expression of Dcx, another member of the doublecortin family of microtubule-associated proteins, is restricted to the brain (Fig. 2 B). We also observed that DCAMKL1 protein levels are elevated during the course of osteoblast differentiation in vitro (Fig. 2 C). Similar to the results in human MSCs, shRNA-mediated reductions in endogenous DCAMKL1 protein levels augmented osteogenesis in mouse osteoblasts (Fig. 2, D–F). When compared with control shRNA targeting GFP, introduction of shRNA specific for *Dcamkl1* into primary osteoblast cultures increased osteoblast-specific gene expression and increased formation of mineralized matrix (Fig. 2, D–F). These results further demonstrate that *Dcamkl1* is expressed within cell types that control bone formation and that differentiation and function of osteoblasts in vitro are sensitive to the endogenous levels of DCAMKL1.

Dcamkl1$^{-/-}$ mice exhibit elevations in bone mass and bone anabolism

Mice deficient in Dcamkl1 have previously been generated and described to be viable and fertile (Deuel et al., 2006; Koizumi et al., 2006). To examine the effect of Dcamkl1 on skeleton development, we first analyzed the growth plate of the *Dcamkl1*$^{-/-}$ mice by hematoxylin and eosin (H&E) staining, revealing that *Dcamkl1*$^{-/-}$ mice have a well-organized growth plate and that the growth plate architecture of these mice is indistinguishable from that of WT controls (Fig. 3 A). To further determine the in vivo effects of Dcamkl1 expression within the skeletal system, we used quantitative computed tomography (µ-QCT) to determine whether differences can be observed in skeletal elements isolated from *Dcamkl1*$^{-/-}$ mice when compared with skeletal elements from WT control mice. As shown in Fig. 3 (B–F), the distal femurs of *Dcamkl1*$^{-/-}$ mice exhibited increases in trabecular bone volume (BV/TV), trabecular number

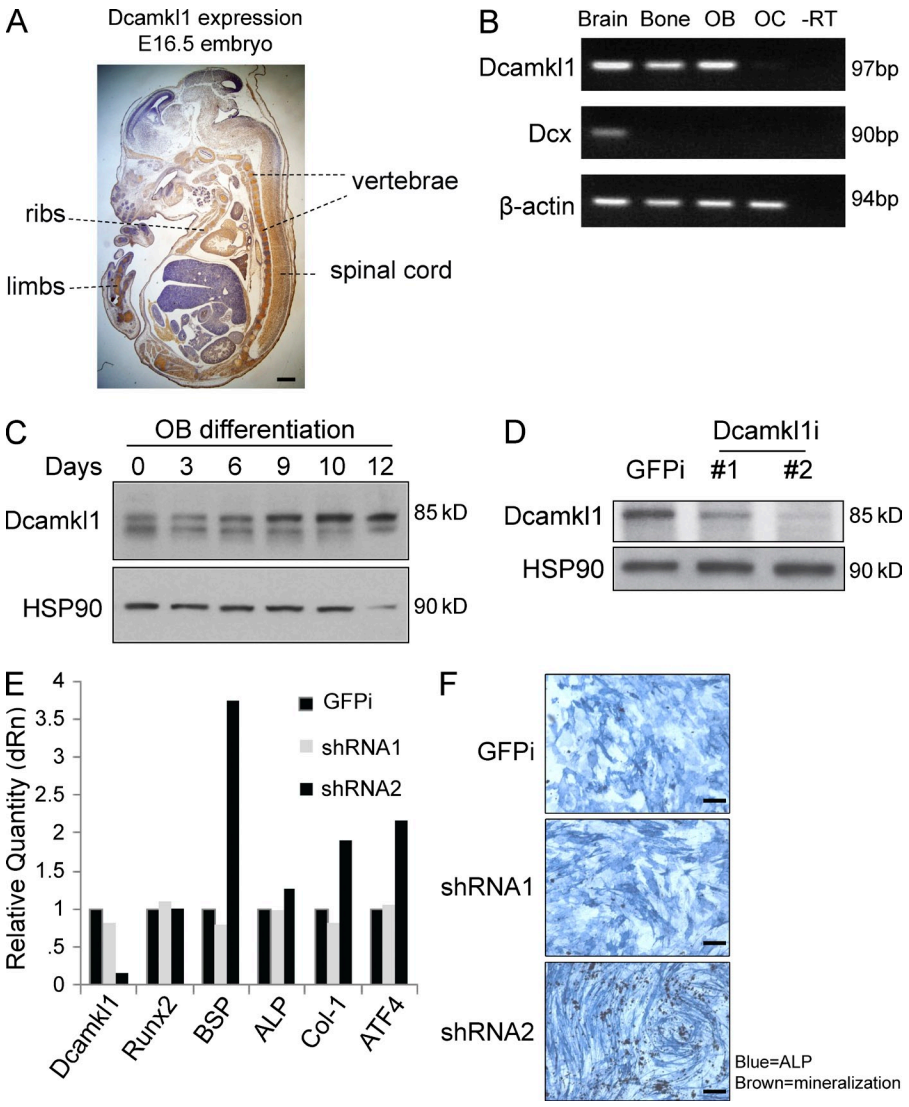

Figure 2. Augmented osteoblast differentiation after silencing of Dcamkl1. (A) Analysis of *Dcamkl1* expression in E16.5 embryos via in situ hybridization. (B) RT-PCR analysis of *Dcamkl1*, *Dcx*, and *β-actin* transcript levels in brain, whole bone, osteoblasts (OB), and osteoclasts (OC). The data are representative of three mice per group and two independent experiments. (C) Analysis of DCAMKL1 protein levels by Western blot over the course of osteoblast differentiation. The data are representative of two independent experiments. (D) Western blot analysis of DCAMKL1 protein levels in osteoblasts that were infected with lentivirus expressing control shRNA or two separate *Dcamkl1*-specific shRNAs. (E) qRT-PCR analysis of osteoblast-specific genes in cells infected with control or *Dcamkl1*-specific shRNAs. (F) Osteoblasts infected with control or *Dcamkl1*-specific shRNAs were cultured for 21 d, and von Kossa staining for mineralization and Fast blue staining for Alp activity were performed. (A, E, and F) The data are representative of three independent experiments. Bars: (A) 100 µm; (F) 20 µm.

(Tb.N), trabecular thickness (Tb.Th), and cortical thickness (C.Th) when compared with the femurs of WT control mice. Given our previous findings that Dcamkl1 can regulate osteoblast differentiation and function in vitro, we used histomorphometric analysis of WT and *Dcamkl1*$^{-/-}$ mice to evaluate static and dynamic parameters of bone formation and resorption (Fig. 3 G and Table 1). Consistent with our µ-QCT data, histomorphometric analysis also demonstrated that *Dcamkl1*$^{-/-}$ mice displayed significant increases in both bone volume (BV/TV) and trabecular thickness (Tb.Th; Fig. 3 G and Table 1). Also, a marked elevation in the number of osteoblasts was observed in tibias isolated from *Dcamkl1*$^{-/-}$ mice (Table 1). To assess whether the increase in osteoblasts is related to expansion of a pool of osteoprogenitor cells, flow cytometric analysis of this population was performed. Recently, a population of osteoprogenitor cells with surface markers CD45^{-} Tie2^{-}αv^{+}CD105^{+}Thy1.2^{-} (CD105^{+}Thy1^{-}) was isolated from bone marrow cells (Chan et al., 2009). This population of cells can produce bone through endochondral ossification. To assess whether there are more osteoprogenitors in the bone marrow of *Dcamkl1*$^{-/-}$ mice, bone cells were isolated from WT and *Dcamkl1*$^{-/-}$ mice and analyzed using flow cytometry. *Dcamkl1* knockout embryos showed similar numbers of CD105^{+}Thy1^{-} osteoprogenitor cells when compared with littermate controls

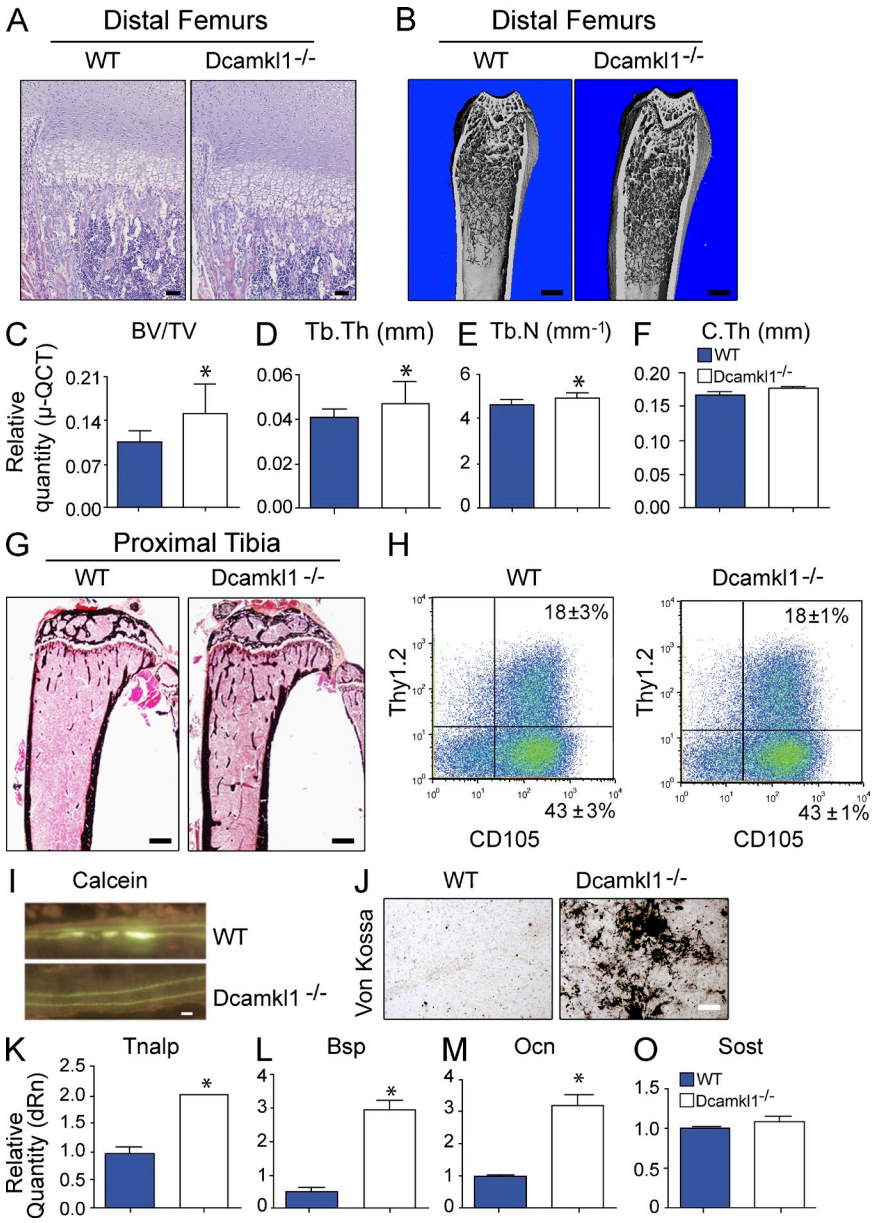

Figure 3. Elevated bone mass present in mice lacking Dcamkl1. (A) H&E staining of distal femur of 4-wk-old WT and *Dcamkl1*$^{-/-}$ mice showing the growth plate architecture of these mice. The data are representative of two independent experiments. (B) 3-D µ-QCT image of distal femurs isolated from 9-wk-old male *Dcamkl1*$^{-/-}$ and WT control mice. (C–F) Analysis of µ-QCT femur images from 9-wk-old male WT and *Dcamkl1*$^{-/-}$ mice for bone volume per tissue volume (BV/TV), trabecular thickness (Tb.Th), trabecular number (Tb.N), and cortical thickness (C.Th). Results are presented as the mean ± SD of six mice per group. (G) von Kossa staining and histomorphometry analysis of proximal tibia from 9-wk-old male *Dcamkl1*$^{-/-}$ and control mice. Results are representative of five mice per group. (H) Representative FACS profiles on pregated, CD45^{-}Ter119^{-} lineage cells harvested from long bone WT and *Dcamkl1* knockout embryos. Percentages represent the percentage of cells within that quadrant. Values are mean ± SD of biological replicates. (I) Dual calcein labeling of tibial bone from WT and *Dcamkl1*$^{-/-}$ mice was visualized by fluorescent microscopy. Results are representative of five mice per group. (J) von Kossa staining of WT and *Dcamkl1*$^{-/-}$ osteoblast cultures at day 16. (K–O) Analysis of *Tnalp* (K), *Bsp* (L), *Ocn* (M), and *Sost* (O) via qPCR in WT and *Dcamkl1*$^{-/-}$ osteoblast cultures. Results are presented as the mean ± SD of triplicates of cells pooled from three mice per group and are representative of two independent experiments. Statistical analysis was performed using an unpaired Student's *t* test: *, $P < 0.05$. Bars: (A) 100 µm; (B and G) 300 µm; (I) 10 µm; (J) 20 µm.

(Fig. 3 H and Fig. S1). Thus, by comparing the number of osteoprogenitors with the results of histomorphometry analysis, we conclude that DCAMKL1 likely functions during osteoblast differentiation, after commitment to the osteoblast lineage. Thus, increased numbers of osteoblasts and enhanced bone formation in *Dcamkl1*$^{-/-}$ mice reflect accelerated osteoblast differentiation, which is consistent with the results of our in vitro knockdown experiments (Fig. 1, D and E; and Fig. 2, D–F).

Table 1. Histomorphometry analysis of *Dcamkl1*$^{-/-}$ mice

Parameter	WT (n = 6)	*Dcamkl1*$^{-/-}$ ($n \geq 5$)	P-value
BV/TV (%)	6.13 ± 0.74	10.39 ± 1.32[a]	0.018
Tb.Th (μm)	28.22 ± 1.01	34.23 ± 1.42[b]	0.006
Tb.N (/mm)	2.18 ± 0.25	3.01 ± 0.29	0.055
Tb.Sp (μm)	464 ± 56	316 ± 39	0.055
MS/BS (%)	36.68 ± 1.80	42.16 ± 1.38[a]	0.045
MAR (μm/d)	1.81 ± 0.05	2.16 ± 0.14[a]	0.033
BFR/BS (μm^3/μm^2/yr)	242 ± 13	331 ± 20[b]	0.004
BFR/BV (%/yr)	1,711 ± 36	2,016 ± 142[a]	0.048
BFR/TV (%/yr)	105 ± 12	184 ± 12[b]	0.001
Ob.S/BS (%)	10.19 ± 2.14	15.55 ± 1.27	0.057
N.Ob/T.Ar (/mm^2)	33.96 ± 5.19	81.52 ± 14.18[a]	0.010
N.Ob/BS (/mm)	8.68 ± 1.62	13.26 ± 1.11[a]	0.042
OS/BS (%)	5.56 ± 1.01	5.88 ± 0.94	0.824
O.Th (μm)	2.49 ± 0.33	2.40 ± 0.29	0.854
Oc.S/BS (%)	0.84 ± 0.21	0.57 ± 0.14	0.303
N.Oc/T.Ar (/mm^2)	1.74 ± 0.59	1.54 ± 0.38	0.783
N.Oc/BS (/mm)	0.37 ± 0.08	0.24 ± 0.06	0.205

Tb.Sp, trabecular separation; N.Ob/T.Ar, osteoblast number/tissue area ratio; N.Ob/BS, osteoblast number/bone surface; N.Oc/T.Ar, osteoclast number/tissue area ratio; N.Oc/BS, osteoclast number/bone surface. 9-wk-old male *Dcamkl1*$^{-/-}$ mice and WT control mice were injected with calcein. 5 d later, mice were injected with calcein again. Mice were sacrificed 3 d after the second injection, and tibias were processed for quantitative histomorphometry. Histomorphometric analysis at proximal tibiae revealed that *Dcamkl1*$^{-/-}$ mice had significantly higher cancellous bone volume and thicker trabeculae than WT controls.

[a]$P < 0.05$ compared with WT, unpaired Student's *t* test.

[b]$P < 0.01$ compared with WT, unpaired Student's *t* test.

Additionally, bone formation rates were elevated in *Dcamkl1*$^{-/-}$ mice compared with control mice. This was caused by an increase in both mineral apposition rate and mineralizing surface as determined by dual-calcein labeling (Fig. 3 I and Table 1). To further verify that the increased bone mass observed in *Dcamkl1*$^{-/-}$ mice is the effect of augmented osteoblast activity, WT and *Dcamkl1*$^{-/-}$ bone marrow stromal cells were differentiated into osteoblasts. The primary osteoblast cultures from *Dcamkl1*$^{-/-}$ mice demonstrated an increased level of mineralized matrix production (Fig. 3 J). Consistent with the enhanced mineralized matrix formation, expression of characteristic osteoblast markers including tissue-nonspecific Alp (Tnalp), bone sialoprotein (Bsp), and osteocalcin (Ocn) were increased in *Dcamkl1*$^{-/-}$ osteoblasts when compared with WT osteoblasts (Fig. 3, K–M).The increased bone mass observed in the *Dcamkl1*$^{-/-}$ mice may be caused by alteration of Wnt–LRP5 pathways. We also examined the expression of the secreted WNT antagonist SOST and did not find obvious difference (Fig. 3 O). These data confirm our previous in vitro observation that *Dcamkl1*-specfic shRNAs can augment osteoblast differentiation and establish that the increased bone mass observed in the *Dcamkl1*$^{-/-}$ mice arises from elevated osteoblast activity.

The increased bone mass present in the long bones of *Dcamkl1*$^{-/-}$ mice could also arise through impaired osteoclast differentiation and/or function. To address this, we analyzed tibias from 4-wk-old WT and *Dcamkl1*$^{-/-}$ mice for the presence of tartrate-resistant acid phosphatase (TRAP)–positive osteoclasts. In comparison with age-matched WT controls, *Dcamkl1*$^{-/-}$ mice showed similar numbers of TRAP-positive cells (Fig. 4, A and B). Further confirming these in vivo findings, bone marrow harvested from *Dcamkl1*$^{-/-}$ mice and cultured in the presence of osteoclast inducers RANKL (receptor activator of NF-κB ligand) and M-CSF resulted in the formation of a similar number of multinucleated TRAP-positive osteoclasts when compared with bone marrow from WT mice (Fig. 4 C). Further analysis of these cultures via quantitative PCR (qPCR) revealed that the osteoclast-specific markers cathepsin K, β3-integrin, and calcitonin receptor were induced to similar levels in WT and *Dcamkl1*$^{-/-}$ cultures when these cells were cultured under conditions that promote osteoclastogenesis (Fig. 4, D–F). Collectively, these results suggest that the elevated bone mass observed in *Dcamkl1*$^{-/-}$ mice is attributed to increased bone formation by osteoblasts as opposed to impaired bone resorption by osteoclasts.

DCAMKL1 regulates the activity of Runx2 in osteoblasts

We next sought to elucidate the mechanism underlying control of osteoblast differentiation by DCAMKL1. Runx2 is a transcription factor essential for osteoblast differentiation and functions. We therefore reasoned that DCAMKL1 might exert its inhibitory influence on osteoblast biology through antagonism of Runx2. To address this question, we asked whether overexpression of DCAMKL1 could alter the ability of Runx2 to activate transcription from the well-characterized OSE2 luciferase reporter construct that contains multimerized Runx2-binding sites (Ducy et al., 1997). As shown in Fig. 5 A, ectopic expression of DCAMKL1 did indeed inhibit Runx2

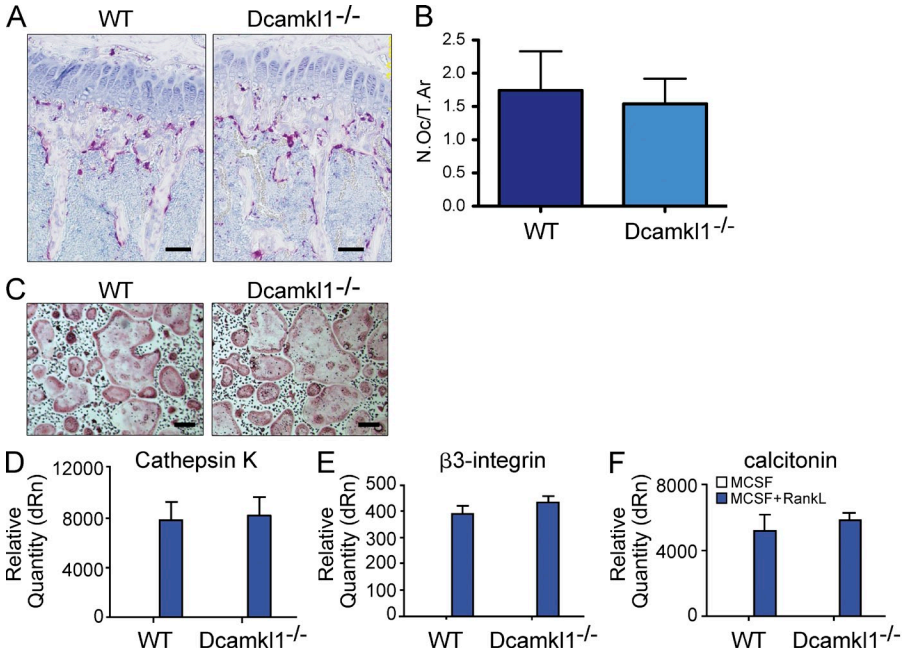

Figure 4. Normal osteoclast differentiation in *Dcamkl1*$^{-/-}$ mice. (A) Histological analysis of TRAP-positive osteoclast populations in the tibia of 4-wk-old male WT and *Dcamkl1*$^{-/-}$ mice. The data are representative of two independent experiments. (B) Histomorphometry analysis of osteoclast surface per tissue area (N.Oc/T.Ar) in the tibia of 9-wk-old male WT control and *Dcamkl1*$^{-/-}$ mice. Results are presented as the mean ± SD of six mice per group. (C) In vitro differentiation of osteoclast precursors from bone marrow cells of WT and *Dcamkl1*$^{-/-}$ mice in the presence M-CSF + RANKL. Cultures were then assayed for the presence of TRAP-positive mature osteoclasts. The data are representative of two independent experiments. Bars: (A) 100 µm; (C) 60 µm. (D–F) qPCR analysis of WT and *Dcamkl1*$^{-/-}$ osteoclast cultures for the expression of cathepsin K (D), β3-integrin (E), and calcitonin receptor (F). Results are presented as the mean ± SD of triplicates of cells pooled from three mice per group and are representative of two independent experiments.

transactivation of this reporter gene. In contrast, DCAMKL1 had no effect on the transcriptional activation of ATF4, another key transcription factor in osteoblast biology (Fig. 5 B). Interestingly, we were unable to detect an association between DCAMKL1 and Runx2 in coimmunoprecipitation experiments (Fig. 5 C), suggesting that the repression of Runx2 function by DCAMKL1 occurs in the absence of a direct interaction between these two proteins.

To gain further insight into how DCAMKL1 controls Runx2 activity, we sought to identify those structural domains of DCAMKL1 that are required to repress Runx2 activity. DCAMKL1 contains a pair of unique doublecortin domains in the N terminus that facilitate its association with microtubules and promote their polymerization (Fig. 5 D; Burgess and Reiner, 2000; Lin et al., 2000). DCAMKL1 also contains a functional Ca^{2+}/calmodulin-dependent (CAM)–like kinase domain in its C terminus, although physiologically relevant substrates for this kinase have yet to be described (Fig. 5 D; Lin et al., 2000; Burgess and Reiner, 2002; Shang et al., 2003). Using a series of truncated mutant proteins of DCAMKL1 in the same luciferase reporter system described above, we found that the inhibitory function of DCAMKL1 requires the presence of the microtubule-associating doublecortin domains (Fig. 5, E and F). As shown in Fig. 5 E, expression of a C-terminal truncated DCAMKL1 mutant containing the doublecortin domains (DCL) retained its ability to repress Runx2 transactivation. In contrast, a truncated DCAMKL1 mutant containing the kinase domain but lacking the doublecortin domains was unable to block transactivation by Runx2 (Fig. 5 E). A full-length DCAMKL1 mutant harboring a point mutation that renders the kinase region nonfunctional but retains its microtubule-polymerizing activity was also capable of inhibiting Runx2 activity in vitro (Fig. 5 F), indicating that DCAMKL1 represses Runx2 through its ability to promote microtubule polymerization, not its kinase activity.

We next questioned whether DCAMKL1 can promote microtubule polymerization in osteoblasts. To address this, osteoblasts were transfected with a construct expressing EGFP or EGFP-tagged DCAMKL1 constructs. Osteoblasts transfected with EGFP-DCAMKL1 formed numerous dendrite-like processes that were rich in DCAMKL1 expression (Fig. 5 H). Staining the cultured cells with anti-tubulin antibody revealed that these dendrite-like processes containing DCAMKL1 were also rich in tubulin (Fig. 5 H). Similar to what was observed with full-length DCAMKL1, transfection of the EGFP-DCL mutant protein that only expresses the doublecortin domain also resulted in the formation of tubulin-rich, dendrite-like processes (Fig. 5 I). As a control, transfection of EGFP or EGFP-CPG16 did not facilitate the formation of tubulin-rich, dendrite-like processes (Fig. 5, G and J). These data demonstrate that the doublecortin domains of DCAMKL1 are required for both microtubule polymerization and for inhibition of Runx2. Given that a previous study has demonstrated that the stabilization of microtubules results in the cytoplasmic

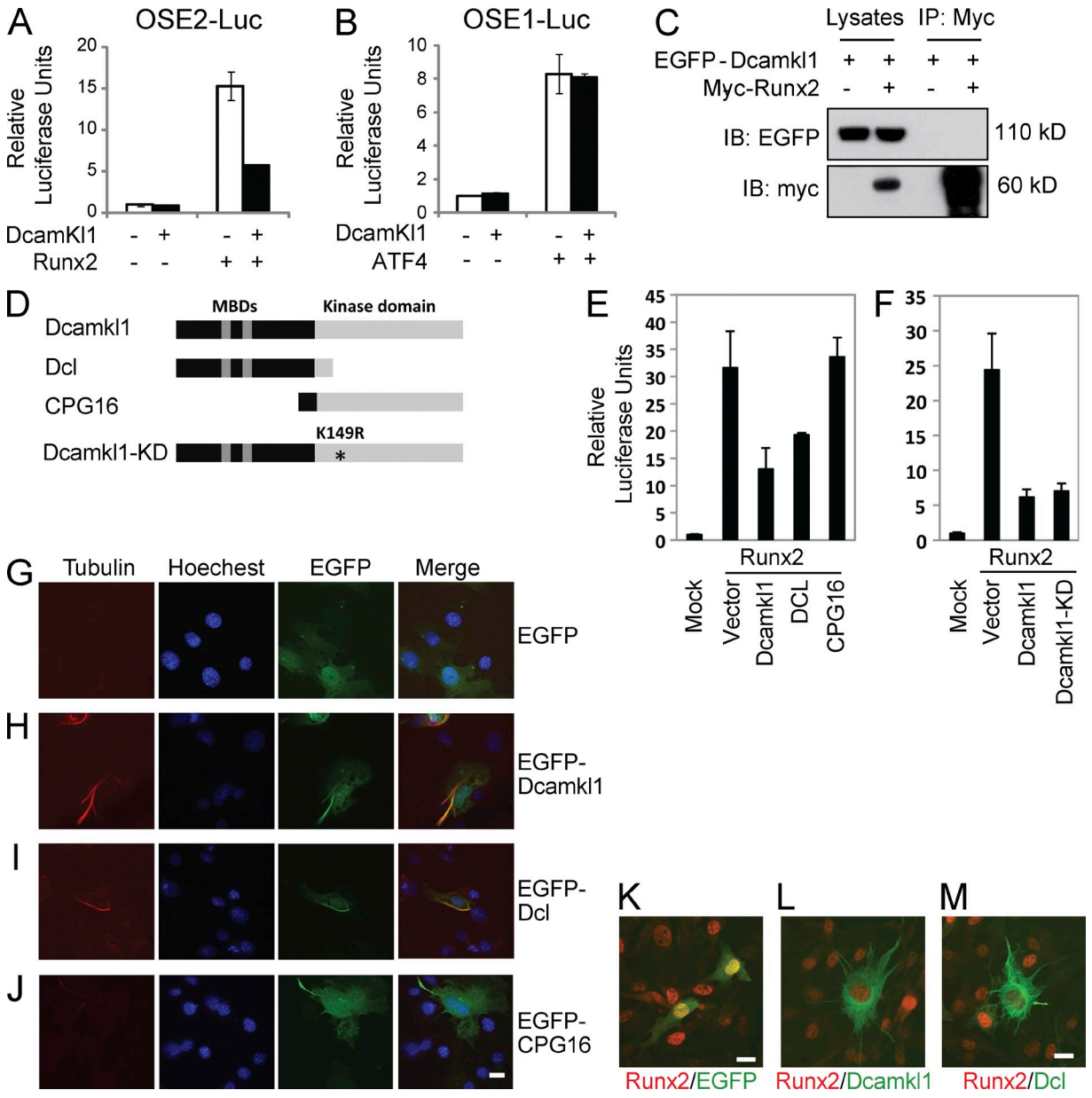

Figure 5. DCAMKL1 regulates microtubule polymerization and Runx2 activity in osteoblast cultures. (A and B) Measurement of Runx2-responsive OSE2 luciferase activity (A) and ATF4-responsive OSE1 luciferase activity (B) in C3H10T1/2 cells with or without DCAMKL1 expression. Results are from lysates harvested from cells 48 h after transfection and were normalized to the expression of the pRL-TK plasmid. Results are presented as the mean ± SD of triplicates of cells and are representative of two independent experiments. (C) The interaction between Runx2 and DCAMKL1 was analyzed by coimmunoprecipitation experiments, which were conducted in 293T cells transfected with Myc-Runx2 and EGFP-Dcamkl1 expression constructs. Runx2 was immunoprecipitated from cell lysates with anti-Myc antibody, followed by Western blot analysis with anti-GFP antibody. IB, immunoblot; IP, immunoprecipitation. (D) Linear schematic of the various Dcamkl1 mutants used in these experiments. MBDs, microtubule-binding domains. (E and F) Measurement of Runx2-responsive OSE2 luciferase activity in C3H10T1/2 cells, which were transfected with the p6xOSE2-Luc reporter plasmids and combinations of Runx2 and different DCAMKL1 expression constructs. Results are presented as the mean ± SD of triplicates of cells and are representative of two independent experiments. (G–J) Staining of cells transfected with constructs expressing EGFP (G), EGFP-DCAMKL1 (H), EGFP-DCL (I), or EGFP-CPG16 (J) with anti-tubulin antibody and Hoechst to visualize microtubules and nuclei, respectively. (K–M) C3H10T1/2 cells were cotransfected with Myc-Runx2 and constructs expressing EGFP (K) and EGFP-Dcamkl1 (L) or EGF-Dcl (M) and were stained with an anti-Myc antibody. Results are representative of two independent experiments. Bars, 10 µm.

sequestration of Runx2 (Pockwinse et al., 2006), we questioned whether DCAMKL1 may repress Runx2 transcriptional activity through sequestering Runx2 in the cytoplasm. To assess this, GFP-tagged DCAMKL1, GFP-tagged DCL mutant, or a control GFP expression vector were transfected into cells expressing myc epitope–tagged Runx2. Analysis of cells transfected with the control GFP expression vector revealed that Runx2 localization was predominantly nuclear

and the subcellular distribution of Runx2 was not perturbed by GFP (Fig. 5 K). Similar to the observation described above, ectopic expression of the full-length DCAMKL1 or the DCL mutant promoted the formation of dendrite-like processes (Fig. 5, L and M). However, Runx2 was still retained in the nucleus of those cells expressing full-length DCAMKL1 or the DCL mutant (Fig. 5, L and M).

Multiple studies have documented that the regulation of Runx2 transcriptional activity is influenced through posttranslational modifications of specific residues within this protein (Bae and Lee, 2006; Jonason et al., 2009). We therefore asked whether DCAMKL1 can alter the phosphorylation pattern of Runx2. For this, we purified Runx2 from 293T cells that either coexpressed DCAMKL1, the DCL mutant of DCAMKL1, or cells treated with the well-characterized microtubule-stabilizing agent taxol (Fig. 6 A). Mass spectroscopy analysis of the purified Runx2 protein revealed that the presence of DCAMKL1 resulted in the phosphorylation of serine residue 125 (Ser125; Fig. 6, B and C). Interestingly, Ser125 phosphorylation is also detectable on Runx2 when it is purified from taxol-treated cells and from cells cotransfected with the DCL mutant of Dcamkl1 but is not detectable in control cells (Fig. 6 B). To further test whether the inhibition of Runx2 by DCAMKL1 is through the phosphorylation of Runx2 at Ser125, we constructed a mutant Runx2 in which Ser125 was mutated to glutamic acid to mimic phosphorylation of Ser125. Strikingly, Runx2 S125E mutation substantially decreased Runx2 activity. More importantly, DCAMKL1 could not further decrease the activity of the Runx2 S125E mutant (Fig. 6 D). A previous study has established that phosphorylation of Ser125 in Runx2 renders Runx2 transcriptionally inert (Phillips et al., 2006). Considering that the microtubule stabilizing agent Taxol could also induce Ser125 phosphorylation, our data support the conclusion that Runx2 inhibition by DCAMKL1 occurs through the induction of microtubule stabilization and the phosphorylation of Runx2 at this negative-regulatory serine residue.

Generation and analysis of Dcamkl1/Runx2 compound mutant mice reveal a genetic interaction in vivo

Based on the in vitro findings described above, we asked whether DCAMKL1 is a bona fide regulator of Runx2 in vivo. *Runx2* haploinsufficiency in humans and mice results in the syndrome cleidocranial dysplasia, which is characterized by the delayed closure of the fontanelles and clavicular hypoplasia (Otto et al., 1997). We postulated that if DCAMKL1 is indeed a negative regulator of Runx2 transcriptional activity, then deletion of *Dcamkl1* in parallel with *Runx2* haploinsufficiency in vivo should lead to amelioration of the skeletal patterning defects observed in $Runx2^{+/-}$ mice. To test this hypothesis, we analyzed skeletal preps generated from WT, $Dcamkl1^{-/-}$, $Runx2^{+/-}$, and $Dcamkl^{-/-}Runx2^{+/-}$ compound mutant mice that were stained with alizarin red and Alcian blue to visualize the various skeletal elements. As shown in Fig. 7 (A–E), $Runx2^{+/-}$ mice display the previously reported cleidocranial dysplasia–like skeletal abnormalities and are also slightly runted when compared with WT and $Dcamkl1^{-/-}$ mice. In contrast, mice with deletions of *Dcamkl1* and heterozygosity for *Runx2* were similar in size to WT mice (Fig. 7, A and B). Furthermore, the hypoplasia of the clavicle in $Runx2^{+/-}$ mice was partially normalized in the $Dcamkl1^{-/-}Runx2^{+/-}$ compound mutant mice (Fig. 7, C and D). $Dcamkl1^{-/-}Runx2^{+/-}$ compound mutant mice also exhibited significant normalization of the calvarial hypomineralization phenotype of $Runx2^{+/-}$ mice (Fig. 7 E). Collectively, these data indicate a genetic interaction between *Dcamkl1* and *Runx2* and provide in vivo verification that DCAMKL1 is a negative regulator of Runx2 within the skeletal system.

DISCUSSION

Although the transcriptional control of anabolic bone formation is an area of active investigation, much remains to be learned about the genetic programs that modulate the function of key transcription factors in osteoblast differentiation and activation. Here we used a functional genomics approach to identify novel regulators of osteogenesis. This forward genetic screen yielded the microtubule-associated protein DCAMKL1 as a previously unrecognized negative regulator of osteoblast differentiation. In vitro and in vivo analyses revealed that DCAMKL1 repressed osteoblast activation by antagonizing Runx2, the master transcription factor in osteoblasts. Introduction of a homozygous *Dcamkl1*-null allele into *Runx2* heterozygous mice reversed aspects of the cleidocranial dysplasia phenotype of these mutant animals. Our results establish a genetic interaction between *Dcamkl1* and *Runx2* in vivo and demonstrate that DCAMKL1 is a physiologically relevant regulator of Runx2-mediated anabolic bone formation. Our study validates the usefulness of a functional genomics approach to discover novel regulators of osteogenesis.

Our findings demonstrate that DCAMKL1 regulates biological processes outside of the central nervous system. Similar to the function of DCAMKL1 in the central nervous system, this protein can also augment microtubule polymerization in osteoblasts. The inhibitory effects of DCAMKL1 on osteoblast differentiation may be explained by its ability to promote microtubule polymerization, a suggestion supported by previous reports demonstrating that treatment of osteoblast cultures with known inhibitors of microtubule assembly can enhance osteoblast differentiation in vitro (Zhao et al., 2009). Furthermore, it has been demonstrated that treatment of mice with these microtubule assembly inhibitors increased bone mass in vivo through augmentation of bone formation rates, mirroring what is observed in $Dcamkl1^{-/-}$ mice (Zhao et al., 2009). In addition to DCAMKL1, other proteins that associate with microtubules are also expressed in osteoblasts (Chiellini et al., 2008). The transcription of *Stathmin-like 2* (*Stmn2*), a member of the stathmin family of cytosolic phosphoproteins, is up-regulated in hMSCs during osteoblast differentiation. However, in contrast to DCAMKL1, stathmins are a class of microtubule accessory proteins that inhibit microtubule polymerization (Curmi et al., 1999). Osteoblast differentiation and function may therefore depend on a precise regulation of multiple proteins that

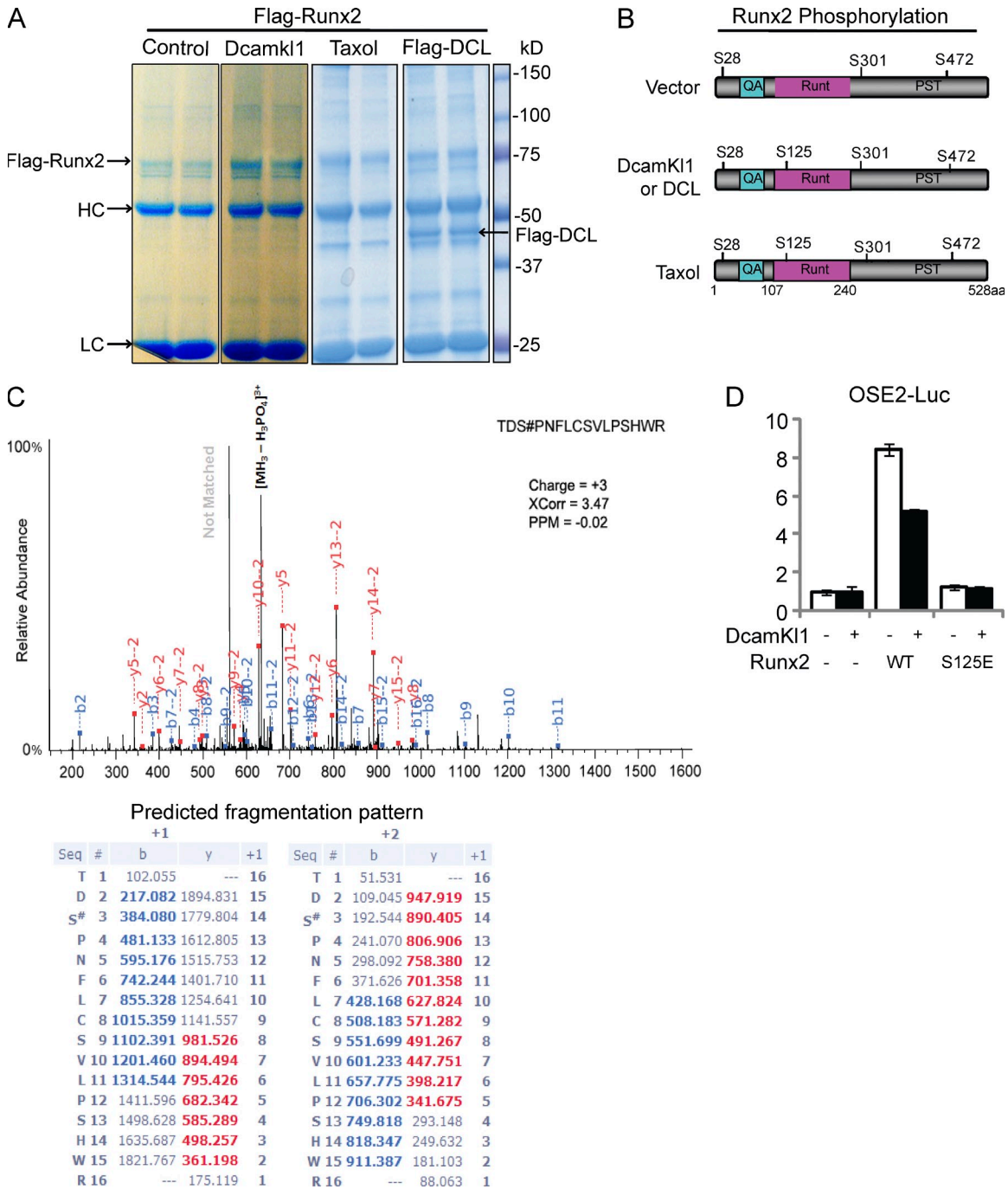

Seq	#	b	y	+1
T	1	102.055	---	16
D	2	217.082	1894.831	15
S#	3	384.080	1779.804	14
P	4	481.133	1612.805	13
N	5	595.176	1515.753	12
F	6	742.244	1401.710	11
L	7	855.328	1254.641	10
C	8	1015.359	1141.557	9
S	9	1102.391	981.526	8
V	10	1201.460	894.494	7
L	11	1314.544	795.426	6
P	12	1411.596	682.342	5
S	13	1498.628	585.289	4
H	14	1635.687	498.257	3
W	15	1821.767	361.198	2
R	16	---	175.119	1

Seq	#	b	y	+1
T	1	51.531	---	16
D	2	109.045	947.919	15
S#	3	192.544	890.405	14
P	4	241.070	806.906	13
N	5	298.092	758.380	12
F	6	371.626	701.358	11
L	7	428.168	627.824	10
C	8	508.183	571.282	9
S	9	551.699	491.267	8
V	10	601.233	447.751	7
L	11	657.775	398.217	6
P	12	706.302	341.675	5
S	13	749.818	293.148	4
H	14	818.347	249.632	3
W	15	911.387	181.103	2
R	16	---	88.063	1

Figure 6. DCAMKL1 regulates Runx2 activity, accompanied by Runx2 Ser125 phosphorylation. (A) Coomassie blue staining of purified Flag-Runx2 protein, which is used for the determination of Runx2 phosphorylation sites by mass spectroscopy. 293T cells were cotransfected with Flag-Runx2 and Dcamkl1 or DCL expression plasmids; after 48 h, Flag-Runx2 protein was purified from 293T cells using M2 beads from Sigma-Aldrich. For the Taxol treatment, the cells were treated with 0.1 µM Taxol for 16 h before harvesting the protein. (B) Schematic indicating the Runx2 phosphorylation sites identified by MS spec analysis. (C) Representative MS/MS spectra for Ser125 phosphorylated TDSPNFLCSVLPSHWR peptide. The mass difference between the peaks corresponds directly to the amino acid sequence. The predicated fragmentation patterns, which are indicated by b ions (blue) and y ions (red), are included to establish a sequence both forward (b ions) and backward (y ions). MS/MS spectra were searched using the SEQUEST algorithm allowing for phosphorylation of serine, threonine, and tyrosine residues. Each spectrum was matched with a q-value of <1%. (D) Effects of Dcamkl1 on WT Runx2 and the Runx2-S125E mutant were assessed by p6xOSE2-Luc reporter in C3H10T1/2 cells. Results are presented as the mean ± SD of triplicates of cells and are representative of two independent experiments.

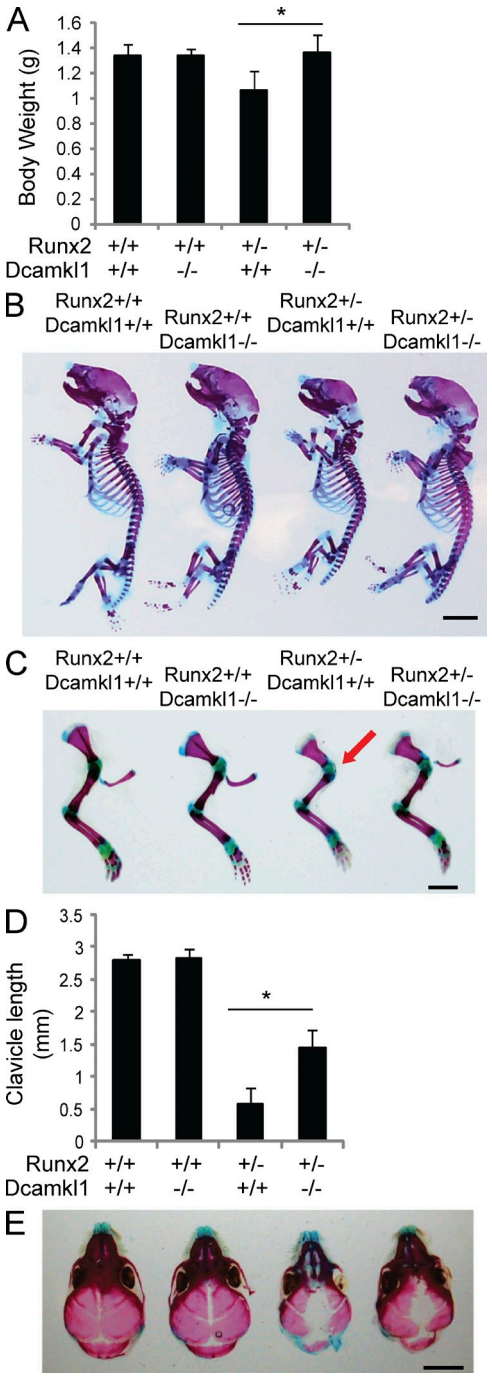

Figure 7. Dcamkl1 genetically interacts with Runx2. (A) Body weight analysis of neonatal WT, *Runx2*$^{+/-}$, *Dcamkl1*$^{-/-}$, and *Dcamkl1*$^{-/-}$*Runx2*$^{+/-}$ mice. Results are presented as the mean ± SD of at least six mice per group. (B, C, and E) Alizarin red– and Alcian blue–stained skeletal preps of P3 WT, *Dcamkl1*$^{-/-}$, *Runx2*$^{+/-}$, and *Dcamkl1*$^{-/-}$*Runx2*$^{+/-}$ mice demonstrates runting (B), clavicular hypoplasia (C), and delayed closure of fontanelles (E) in *Runx2*$^{+/-}$ mice. The red arrow in C indicates the presence of a short clavicle. Results are representative of at least four mice per group. Bars: (B) 600 µm; (C) 300 µm; (E) 500 µm. (D) The clavicle length of p3 WT, *Dcamkl1*$^{-/-}$, *Runx2*$^{+/-}$, and *Dcamkl1*$^{-/-}$*Runx2*$^{+/-}$ mice was quantified. Results are presented as the mean ± SD of at least eight mice per group. Statistical analysis was performed using an unpaired Student's *t* test: *, $P < 0.001$.

control the dynamic nature of microtubule polymerization and depolymerization.

We further demonstrate that DCAMKL1 antagonizes the activity of Runx2 in a transient reporter assay. We found that the ability of DCAMKL1 to repress Runx2 transcriptional activity required the Doublecortin domains of DCAMKL1. The Doublecortin domains are required for the microtubule-polymerizing activity of DCAMKL1, suggesting that Runx2 activity may be sensitive to active polymerization of microtubules. Coexpression of DCAMKL1 with Runx2 resulted in phosphorylation of Runx2 at Ser125. A previous study has demonstrated that phosphorylation of this serine residue inhibits Runx2 activity (Phillips et al., 2006). Mutation of the corresponding serine residue in human Runx2 has also been identified in a patient with cleidocranial dysplasia, suggesting that phosphorylation of this residue can influence Runx2 activity in vitro and in vivo (Wee et al., 2002). Although DCAMKL1 contains a functional kinase domain, phosphorylation of Ser125 on Runx2 was also observed in cells transfected with the DCL mutant, suggesting that the microtubule-stabilizing function of DCAMKL1 is necessary for its ability to induce phosphorylation of Runx2. Furthermore, phosphorylation of Runx2 at Ser125 could be promoted by taxol, a microtubule-stabilizing agent. Understanding how DCAMKL1-mediated microtubule polymerization promotes the phosphorylation of Runx2 is an area of active investigation. It has been established that microtubules can facilitate signaling from the cell surface to the nucleus through retrograde transport of kinases (Moises et al., 2007). Therefore, stabilization of microtubules by DCAMKL1 within osteoblasts may facilitate the localization of certain kinases in the nucleus that promote Runx2 phosphorylation.

A previous study has demonstrated that DCAMKL1 regulates the transition from prometaphase to metaphase through a process that also requires its doublecortin domains (Shu et al., 2006). DCAMKL1 may therefore alter osteoblast differentiation through affecting cell cycle progression. Indeed, commitment of MSCs to the osteoblast lineage requires exiting from the cell cycle, a process which is mediated by Runx2 (Pratap et al., 2003). Altering the DNA-binding and transcriptional activity of Runx2 at various stages of the cell cycle may dictate the stage-specific expression of genes that are essential for driving osteoblast lineage commitment (Qiao et al., 2006). This oscillation of microtubule polymerization and depolymerization, mediated by various mitogen-activated proteins (MAPs) such as DCAMKL1 may coordinate cell cycle with Runx2 transcriptional activity.

Through the generation and analysis of Dcamkl1/Runx2 compound mutant mice, we established that the cleidocranial dysplasia phenotype observed in *Runx2*$^{+/-}$ mice can be partially reversed by deletion of *Dcamkl1* and provided in vivo evidence that *Dcamkl1* is a bona fide regulator of Runx2. In addition to regulating osteoblast lineage commitment, Runx2 has also been reported to regulate chondrocyte maturation as well. To examine the effect of *Dcamkl1* on chondrocyte development, we analyzed the growth plate of the *Dcamkl1*$^{-/-}$ mice by Safranin O staining and H&E staining (Fig. 3 A and

not depicted), revealing that *Dcamkl1*$^{-/-}$ mice have a well-organized growth plate and that the growth plate architecture of these mice is indistinguishable from that of WT controls. The absence of a growth plate phenotype in the *Dcamkl1*-null mice may result from compensatory mechanisms that arise between DCAMKL1 and other microtubule-associated proteins expressed in these tissues. Interestingly, another member of the doublecortin family of microtubule-associated proteins, DCX, is expressed in chondrocytes (Zhang et al., 2007). Within the central nervous system, significant overlap in the expression of DCAMKL1 and DCX results in a functional redundancy that masks specific phenotypes in the central nervous system that are only observed in Dcamkl1/Dcx compound mutant mice (Deuel et al., 2006; Koizumi et al., 2006; Shu et al., 2006). It is possible that the analysis of mice deficient in both Dcamkl1 and Dcx may reveal additional skeletal phenotypes, further expanding the functions of the microtubule-associated proteins to cell populations outside of the osteoblast.

MATERIALS AND METHODS

Mouse mutants. Compound *Dcamkl1/Runx2* mutant mice were generated using the previously described strains of *Dcamkl1*$^{-/-}$ mice and *Runx2*$^{+/-}$ mice (Mundlos et al., 1997; Otto et al., 1997; Deuel et al., 2006). Animals were maintained in accordance with the National Institutes of Health Guide for the Care and Use of Laboratory Animals and were handled according to protocols approved by the institution's subcommittee on animal care (IACUC).

shRNA screen. For the in vitro osteoblast differentiation screen, hMSCs (Lonza) were maintained and expanded according to the manufacturer's instructions. For the entire primary and secondary screen, we used hMSCs from the same lot and passage to minimize variability. MSCs were seeded at a specific density in Optilux 96-well plates (BD) in MSC growth media (MSGM) and rested overnight. Each well was infected with an individual lentiviral clone that expresses a specific and unique shRNA along with a puromycin resistance gene. In addition to the ∼8,000 hairpins corresponding to 1,500 genes, the screen also included a control 96-well plate that consisted of 90 individual shRNAs directed against GFP, RFP, luciferase, or β-galactosidase. Cells that had been successfully infected with the lentiviral clone were selected after puromycin treatment and cultured for an additional 4 d. Osteoblast differentiation was assessed by measuring levels of Alp. Given the variability in viral titer and rate of infection, the level of Alp in a given well was normalized to cell number as quantified by the Alamar blue assay (Invitrogen). For this assay, cells were cultured in media containing Alamar blue for ∼4 h at 37°C. Plates were read on a fluorometer at 570 nm. Media containing Alamar blue was removed, and cells were washed once with sterile PBS. Cells were then incubated with 6.5 mM Na_2CO_3, 18.5 mM $NaHCO_3$, 2 mM $MgCl_2$, and Alp substrate (Sigma-Aldrich) for 1 h at room temperature. After the incubation period, the plate was read with a luminometer (Thermo Fisher Scientific) at 405 nm. The Alp data were plotted versus the Alamar blue data to generate an XY scatter plot (Fig. 1 C), and a second-order polynomial was used to describe a best-fit line for the XY scatter plot. From this best fit line, a predicted Alp value is generated for each individual Alamar blue reading. An API, generated by dividing the actual Alp level by the expected Alp level and then multiplying by 100 [API = (actual AP/expected AP) × 100)], was assigned to each sample. A mean API and standard deviation were then generated for the entire population. A list of candidates was identified in the primary screen based on the API of known genes that regulate MSC differentiation. We further validated these candidates by rescreening the 750 shRNAs corresponding to the 150 target genes that were identified by the primary screen. To decrease the possibility of false positives, candidates that passed the second screen were further validated in MSCs derived from two additional donors.

Immunohistochemistry and in situ hybridization. Mouse embryos and tissues were fixed in 4% paraformaldehyde (PFA) and embedded in paraffin. For in situ hybridization, a DIG labeling kit (Roche) was used to label digoxigenin (DIG) probes as per the manufacturer's instructions. In brief, DIG-labeled antisense probes were prepared with T7 RNA polymerase to detect Dcamkl1 mRNA expression. Probes for Dcamkl1 were amplified from primary mouse osteoblast cDNA using the following primers: Dcamkl1-5′, 5′-AAGTCAGTACCAGCAAGTCTCC-3′; and Dcamkl1-3′-T7, 5′-TTGTAATACGACTCACTATAGGGGCTGCAGATCAGTGTAGAGTTCG-3′. Probes were purified by washing over an Ultrafree-MC filter column (EMD Millipore). Tissue sections were prewarmed at 55°C and deparaffinized and rehydrated by passage through xylene and 100, 95, and 70% ethanol. To quench endogenous peroxidase activity, sections were incubated in 3% hydrogen peroxide for 15 min. Samples were then treated with 10 µg/ml proteinase K for 15 min, 4% PFA for 5 min, and 0.25% acetic acid for 15 min before being dehydrated by passage through increasing concentrations of ethanol. Probe was added to the hybridization solution (50% formamide, 10 mM Tris-HCl, pH 7.5, 200 µg/ml tRNA, 1× Denhardt's, 10% dextran sulfate, 600 mM NaCl, 0.25% SDS, and 1 mM EDTA), and the solution was prewarmed to 85°C before incubation with the tissue sections overnight. After incubation, sections were washed with standard Na citrate buffer and treated with 10 µg/ml RNase A in TNE buffer (10 mM Tris-HCl, 100 mM NaCl, and 1 mM EDTA). DIG-labeled probe was then detected by immunostaining with anti–DIG-POD and streptavidin–horseradish peroxidase. The enzyme reaction was stopped by water, and the slides were counterstained in hematoxylin and dehydrated and mounted in xylene-based media.

Skeletal preparation and staining. Mice were skinned, eviscerated, and dehydrated in 95% EtOH overnight. The samples were then transferred into acetone for an additional 48-h incubation. Skeletal preparations were stained for 2 d using Alcian blue and alizarin red as described previously (McLeod, 1980). After staining, the samples were washed three times for 30 min in 95% EtOH. Soft tissue was then cleared in 1% KOH.

Micro-computed tomography (µCT) analysis. Femurs were isolated from 9-wk-old male WT and Dcamkl1$^{-/-}$ mice and fixed in 70% EtOH. A region 0.28 mm proximal to the distal growth plate was scanned using a µCT 35 system (Scanco Medical) with a spatial resolution of 7 µm. From these scans, a region of 2.1 mm in length of the distal metaphysis was selected for analysis. Images were reconstructed into three-dimensional (3-D) volumes with the region of interest being segmented using a fixed threshold. Unbiased, 3-D microstructural properties of trabecular bone, including bone volume fraction (BV/TV), trabecular thickness (Tb.Th), trabecular number (Tb.N), cortical thickness (C.Th), were then calculated for the trabecular region of the metaphysis of the distal femur using methods based on distance transformation of the binarized images (Hildebrand and Rüegsegger, 1997).

Bone histomorphometry. 9-wk-old male WT and Dcamkl1$^{-/-}$ mice were intraperitoneally injected with 20 mg/kg calcein on days 8 and 3 before necropsy. Tibiae were removed, dehydrated in ethanol, infiltrated, and embedded without demineralization in methyl methacrylate. Undecalcified sections were cut at a thickness of 5 µm and mounted unstained for dynamic measurements. Consecutive sections were stained with toluidine blue to quantitate bone cell measurements. Histomorphometric analysis was performed using the OsteoMeasure system (Osteometrics, Inc.), and the results were expressed according to standardized nomenclature (Parfitt et al., 1987). A sampling site with an area of ∼1.2 mm^2 was established in the secondary spongiosa of the metaphysis. The dynamic measurements included mineral apposition rate (MAR), mineralizing surface (MS/BS), and bone formation rate expressed per bone surface referent (BFR/BS), bone volume referent (BFR/BV), and tissue volume referent (BFR/TV). Osteoblast surface (Ob.S/BS) and osteoclast surface (Oc.S/BS) were determined as trabecular surface covered by large basophilic cuboidal cells and multinucleated (two or more nuclei) cells, respectively. Osteoblast number (N.Ob) and osteoclast number (N.Oc) were counted and expressed per bone perimeter (B.Pm) and tissue area (T.Ar). Osteoid surface (OS/BS) and osteoid thickness (O.Th) were also measured.

Primary cell culture. Osteoblastic cells were isolated from calvariae of neonatal WT and *Dcamkl1*$^{-/-}$ littermates as previously described (Jones et al., 2006). Calvarial-derived cells were plated in α-MEM + 10% FBS in a 6-well dish. Cells were harvested at a subconfluent stage and replated in a 6-well dish at a concentration of 10^4 cells/cm^2 in α-MEM + 10% FBS + 50 µg/ml ascorbic acid + 5 mM β-glycerophosphate. For von Kossa staining, cells were fixed at day 21 of culture with 10% neutral buffered formalin and stained with 5% silver nitrate for 30 min. For Alp, cultures were fixed in 100% ethanol at day 14 of culture and stained using an Alp kit (Sigma-Aldrich) per the manufacturer's instructions.

For in vitro osteoclastogenesis, bone marrow cells were isolated from the femur and tibia of mice in α-MEM (Corning). After red blood cell lysis, cells were washed once and resuspended in α-MEM + 10% FBS and plated in a 48-well plate at a concentration of 2×10^5 cells per 250 µl of α-MEM + 10% FBS. Cells were cultured for 2 d in the presence of 50 ng/ml M-CSF (PeproTech) followed by an additional 5 d in the presence of 50 ng/ml M-CSF and either 25 or 100 ng/ml RANKL (PeproTech). The cells were then fixed and stained for the presence of TRAP using a kit per the manufacturer's instructions (Sigma-Aldrich).

Transient transfections and reporter gene assays. The mouse MSC line C3H10T1/2 was maintained in DMEM (Corning) + 10% FBS. For transient transfections, cells were seeded overnight in a 12-well dish at a concentration of 8×10^4 cells/well. Cells were then transfected with a luciferase reporter gene plasmid and varied combinations of expression constructs, as indicated, using Effectene transfection reagent (QIAGEN). Total amounts of transfected DNA were kept constant by supplementing with control empty expression vector plasmids as needed. All cells were cotransfected with pRL-TK (Promega) as a normalization control for transfection efficiency. 48 h after transfection, cells were harvested and lysed in 1× Passive Lysis Buffer (Promega). Luciferase assays were performed using the Dual-Luciferase Reporter Assay System (Promega). All luciferase experiments were repeated at least three times. C. Walsh (Beth Israel Deaconess Medical Center, Boston, MA) and L.-H. Tsai (Harvard Medical School, Boston, MA) provided the Dcamkl1 expression plasmids. The Runx2 expression plasmids were the gift of G. Karsenty (Columbia University, New York, NY). The multimerized OSE luciferase (6xOSE2) construct was obtained from B. Olsen (Harvard School of Dental Medicine, Boston, MA).

Mass spectrometry. For phosphorylation site mapping on Runx2, purified Runx2 protein was resolved on SDS-PAGE and visualized by colloidal Coomassie blue. The band containing Runx2 was excised and treated with DTT to reduce disulfide bonds and iodoacetamide to derivatize cysteine residues. The protein was digested in gel by using trypsin and then analyzed by nanoscale-microcapillary reversed phase liquid chromatography tandem mass spectrometry (LC-MS/MS) as described previously (Villén and Gygi, 2008). MS/MS spectra were searched using the SEQUEST algorithm (Eng et al., 1994) against a database containing the sequences of hRunx2 and common contaminants such as human keratin proteins with static modifications of cysteine carboxymethylation, dynamic modification of methionine oxidation, and serine, threonine, and tyrosine phosphorylation. All peptide matches were filtered based on mass deviation, tryptic state, and XCorr and were confirmed by manual validation.

Online supplemental material. Fig. S1 shows a representative FACS profile of homogenized E17.5 long bone pregated for live CD45$^-$Ter119$^-$ cells showing CD105$^+$Thy1.2$^-$, CD105$^+$Thy1.2$^+$. Online supplemental material is available at http://www.jem.org/cgi/content/full/jem.20111790/DC1.

We thank Drs. Christopher Walsh, Gerard Karsenty, Li-Huei Tsai, and Bjorn Olsen for kindly providing reagents. We thank Dorothy Zhang Hu for technical assistance in histology analysis. We also thank Drs. Nir Hacohen, Serena Silver, and David Root at the Broad Institute's RNAi Platform for technical assistance and reagents.

This work is supported by National Institutes of Health grants HD055601 (to L.H. Glimcher) and K99AR055668 (to D.C. Jones) and a grant from Merck Pharmaceuticals. W. Zou is a recipient of the Thousand Young Talents Program of the Chinese government.

The authors have no competing financial interests.

Submitted: 25 August 2011
Accepted: 3 July 2013

REFERENCES

Bae, S.C., and Y.H. Lee. 2006. Phosphorylation, acetylation and ubiquitination: the molecular basis of RUNX regulation. *Gene*. 366:58–66. http://dx.doi.org/10.1016/j.gene.2005.10.017

Boyle, W.J., W.S. Simonet, and D.L. Lacey. 2003. Osteoclast differentiation and activation. *Nature*. 423:337–342. http://dx.doi.org/10.1038/nature01658

Burgess, H.A., and O. Reiner. 2000. Doublecortin-like kinase is associated with microtubules in neuronal growth cones. *Mol. Cell. Neurosci.* 16:529–541. http://dx.doi.org/10.1006/mcne.2000.0891

Burgess, H.A., and O. Reiner. 2002. Alternative splice variants of doublecortin-like kinase are differentially expressed and have different kinase activities. *J. Biol. Chem.* 277:17696–17705. http://dx.doi.org/10.1074/jbc.M111981200

Burgess, H.A., S. Martinez, and O. Reiner. 1999. KIAA0369, doublecortin-like kinase, is expressed during brain development. *J. Neurosci. Res.* 58:567–575. http://dx.doi.org/10.1002/(SICI)1097-4547(19991115)58:4<567::AID-JNR9>3.0.CO;2-T

Chan, C.K., C.C. Chen, C.A. Luppen, J.B. Kim, A.T. DeBoer, K. Wei, J.A. Helms, C.J. Kuo, D.L. Kraft, and I.L. Weissman. 2009. Endochondral ossification is required for haematopoietic stem-cell niche formation. *Nature*. 457:490–494. http://dx.doi.org/10.1038/nature07547

Chiellini, C., G. Grenningloh, O. Cochet, M. Scheideler, Z. Trajanoski, G. Ailhaud, C. Dani, and E.Z. Amri. 2008. Stathmin-like 2, a developmentally-associated neuronal marker, is expressed and modulated during osteogenesis of human mesenchymal stem cells. *Biochem. Biophys. Res. Commun.* 374:64–68. http://dx.doi.org/10.1016/j.bbrc.2008.06.121

Curmi, P.A., O. Gavet, E. Charbaut, S. Ozon, S. Lachkar-Colmerauer, V. Manceau, S. Siavoshian, A. Maucuer, and A. Sobel. 1999. Stathmin and its phosphoprotein family: general properties, biochemical and functional interaction with tubulin. *Cell Struct. Funct.* 24:345–357. http://dx.doi.org/10.1247/csf.24.345

Deuel, T.A., J.S. Liu, J.C. Corbo, S.Y. Yoo, L.B. Rorke-Adams, and C.A. Walsh. 2006. Genetic interactions between doublecortin and doublecortin-like kinase in neuronal migration and axon outgrowth. *Neuron*. 49:41–53. http://dx.doi.org/10.1016/j.neuron.2005.10.038

Ducy, P., R. Zhang, V. Geoffroy, A.L. Ridall, and G. Karsenty. 1997. Osf2/Cbfa1: a transcriptional activator of osteoblast differentiation. *Cell*. 89:747–754. http://dx.doi.org/10.1016/S0092-8674(00)80257-3

Eng, J.K., A.L. McCormack, and J.R. Yates III. 1994. An approach to correlate tandem mass spectral data of peptides with amino acid sequences in a protein database. *J. Am. Soc. Mass Spectrom.* 5:976–989. http://dx.doi.org/10.1016/1044-0305(94)80016-2

Erlebacher, A., E.H. Filvaroff, S.E. Gitelman, and R. Derynck. 1995. Toward a molecular understanding of skeletal development. *Cell*. 80:371–378. http://dx.doi.org/10.1016/0092-8674(95)90487-5

Gerbe, F., B. Brulin, L. Makrini, C. Legraverend, and P. Jay. 2009. DCAMKL-1 expression identifies Tuft cells rather than stem cells in the adult mouse intestinal epithelium. *Gastroenterology*. 137:2179–2180. http://dx.doi.org/10.1053/j.gastro.2009.06.072

Harada, S., and G.A. Rodan. 2003. Control of osteoblast function and regulation of bone mass. *Nature*. 423:349–355. http://dx.doi.org/10.1038/nature01660

Hildebrand, T., and P. Rüegsegger. 1997. A new method for the model-independent assessment of thickness in three-dimensional images. *J. Microsc.* 185:67–75. http://dx.doi.org/10.1046/j.1365-2818.1997.1340694.x

Itzkovitz, S., A. Lyubimova, I.C. Blat, M. Maynard, J. van Es, J. Lees, T. Jacks, H. Clevers, and A. van Oudenaarden. 2012. Single-molecule transcript counting of stem-cell markers in the mouse intestine. *Nat. Cell Biol.* 14:106–114. http://dx.doi.org/10.1038/ncb2384

Jonason, J.H., G. Xiao, M. Zhang, L. Xing, and D. Chen. 2009. Post-translational regulation of Runx2 in bone and cartilage. *J. Dent. Res.* 88:693–703. http://dx.doi.org/10.1177/0022034509341629

Jones, D.C., M.N. Wein, M. Oukka, J.G. Hofstaetter, M.J. Glimcher, and L.H. Glimcher. 2006. Regulation of adult bone mass by the zinc finger adapter protein Schnurri-3. *Science.* 312:1223–1227. http://dx.doi.org/10.1126/science.1126313

Karsenty, G., and E.F. Wagner. 2002. Reaching a genetic and molecular understanding of skeletal development. *Dev. Cell.* 2:389–406. http://dx.doi.org/10.1016/S1534-5807(02)00157-0

Kim, S.Y., I.F. Dunn, R. Firestein, P. Gupta, L. Wardwell, K. Repich, A.C. Schinzel, B. Wittner, S.J. Silver, D.E. Root, et al. 2010. CK1epsilon is required for breast cancers dependent on beta-catenin activity. *PLoS ONE.* 5:e8979. http://dx.doi.org/10.1371/journal.pone.0008979

Koizumi, H., T. Tanaka, and J.G. Gleeson. 2006. Doublecortin-like kinase functions with doublecortin to mediate fiber tract decussation and neuronal migration. *Neuron.* 49:55–66. http://dx.doi.org/10.1016/j.neuron.2005.10.040

Komori, T., H. Yagi, S. Nomura, A. Yamaguchi, K. Sasaki, K. Deguchi, Y. Shimizu, R.T. Bronson, Y.H. Gao, M. Inada, et al. 1997. Targeted disruption of Cbfa1 results in a complete lack of bone formation owing to maturational arrest of osteoblasts. *Cell.* 89:755–764. http://dx.doi.org/10.1016/S0092-8674(00)80258-5

Lian, J.B., G.S. Stein, A. Javed, A.J. van Wijnen, J.L. Stein, M. Montecino, M.Q. Hassan, T. Gaur, C.J. Lengner, and D.W. Young. 2006. Networks and hubs for the transcriptional control of osteoblastogenesis. *Rev. Endocr. Metab. Disord.* 7:1–16. http://dx.doi.org/10.1007/s11154-006-9001-5

Lin, P.T., J.G. Gleeson, J.C. Corbo, L. Flanagan, and C.A. Walsh. 2000. DCAMKL1 encodes a protein kinase with homology to doublecortin that regulates microtubule polymerization. *J. Neurosci.* 20:9152–9161.

Martin, T., J.H. Gooi, and N.A. Sims. 2009. Molecular mechanisms in coupling of bone formation to resorption. *Crit. Rev. Eukaryot. Gene Expr.* 19:73–88. http://dx.doi.org/10.1615/CritRevEukarGeneExpr.v19.i1.40

Matsumoto, N., D.T. Pilz, and D.H. Ledbetter. 1999. Genomic structure, chromosomal mapping, and expression pattern of human DCAMKL1 (KIAA0369), a homologue of DCX (XLIS). *Genomics.* 56:179–183. http://dx.doi.org/10.1006/geno.1998.5673

May, R., T.E. Riehl, C. Hunt, S.M. Sureban, S. Anant, and C.W. Houchen. 2008. Identification of a novel putative gastrointestinal stem cell and adenoma stem cell marker, doublecortin and CaM kinase-like-1, following radiation injury and in adenomatous polyposis coli/multiple intestinal neoplasia mice. *Stem Cells.* 26:630–637. http://dx.doi.org/10.1634/stemcells.2007-0621

McLeod, M.J. 1980. Differential staining of cartilage and bone in whole mouse fetuses by alcian blue and alizarin red S. *Teratology.* 22:299–301. http://dx.doi.org/10.1002/tera.1420220306

Moffat, J., D.A. Grueneberg, X. Yang, S.Y. Kim, A.M. Kloepfer, G. Hinkle, B. Piqani, T.M. Eisenhaure, B. Luo, J.K. Grenier, et al. 2006. A lentiviral RNAi library for human and mouse genes applied to an arrayed viral high-content screen. *Cell.* 124:1283–1298. http://dx.doi.org/10.1016/j.cell.2006.01.040

Moises, T., A. Dreier, S. Flohr, M. Esser, E. Brauers, K. Reiss, D. Merken, J. Weis, and A. Krüttgen. 2007. Tracking TrkA's trafficking: NGF receptor trafficking controls NGF receptor signaling. *Mol. Neurobiol.* 35:151–159. http://dx.doi.org/10.1007/s12035-007-8000-1

Mundlos, S., F. Otto, C. Mundlos, J.B. Mulliken, A.S. Aylsworth, S. Albright, D. Lindhout, W.G. Cole, W. Henn, J.H. Knoll, et al. 1997. Mutations involving the transcription factor CBFA1 cause cleidocranial dysplasia. *Cell.* 89:773–779. http://dx.doi.org/10.1016/S0092-8674(00)80260-3

Omori, Y., M. Suzuki, K. Ozaki, Y. Harada, Y. Nakamura, E. Takahashi, and T. Fujiwara. 1998. Expression and chromosomal localization of KIAA0369, a putative kinase structurally related to Doublecortin. *J. Hum. Genet.* 43:169–177. http://dx.doi.org/10.1007/s100380050063

Otto, F., A.P. Thornell, T. Crompton, A. Denzel, K.C. Gilmour, I.R. Rosewell, G.W. Stamp, R.S. Beddington, S. Mundlos, B.R. Olsen, et al. 1997. Cbfa1, a candidate gene for cleidocranial dysplasia syndrome, is essential for osteoblast differentiation and bone development. *Cell.* 89:765–771. http://dx.doi.org/10.1016/S0092-8674(00)80259-7

Parfitt, A.M., M.K. Drezner, F.H. Glorieux, J.A. Kanis, H. Malluche, P.J. Meunier, S.M. Ott, and R.R. Recker; Report of the ASBMR Histomorphometry Nomenclature Committee. 1987. Bone histomorphometry: standardization of nomenclature, symbols, and units. *J. Bone Miner. Res.* 2:595–610. http://dx.doi.org/10.1002/jbmr.5650020617

Phillips, J.E., C.A. Gersbach, A.M. Wojtowicz, and A.J. García. 2006. Glucocorticoid-induced osteogenesis is negatively regulated by Runx2/Cbfa1 serine phosphorylation. *J. Cell Sci.* 119:581–591. http://dx.doi.org/10.1242/jcs.02758

Pockwinse, S.M., A. Rajgopal, D.W. Young, K.A. Mujeeb, J. Nickerson, A. Javed, S. Redick, J.B. Lian, A.J. van Wijnen, J.L. Stein, et al. 2006. Microtubule-dependent nuclear-cytoplasmic shuttling of Runx2. *J. Cell. Physiol.* 206:354–362. http://dx.doi.org/10.1002/jcp.20469

Pratap, J., M. Galindo, S.K. Zaidi, D. Vradii, B.M. Bhat, J.A. Robinson, J.Y. Choi, T. Komori, J.L. Stein, J.B. Lian, et al. 2003. Cell growth regulatory role of Runx2 during proliferative expansion of preosteoblasts. *Cancer Res.* 63:5357–5362.

Qiao, M., P. Shapiro, M. Fosbrink, H. Rus, R. Kumar, and A. Passaniti. 2006. Cell cycle-dependent phosphorylation of the RUNX2 transcription factor by cdc2 regulates endothelial cell proliferation. *J. Biol. Chem.* 281:7118–7128. http://dx.doi.org/10.1074/jbc.M508162200

Shang, L., Y.G. Kwon, S. Nandy, D.S. Lawrence, and A.M. Edelman. 2003. Catalytic and regulatory domains of doublecortin kinase-1. *Biochemistry.* 42:2185–2194. http://dx.doi.org/10.1021/bi026913i

Shu, T., H.C. Tseng, T. Sapir, P. Stern, Y. Zhou, K. Sanada, A. Fischer, F.M. Coquelle, O. Reiner, and L.H. Tsai. 2006. Doublecortin-like kinase controls neurogenesis by regulating mitotic spindles and M phase progression. *Neuron.* 49:25–39. http://dx.doi.org/10.1016/j.neuron.2005.10.039

Sossey-Alaoui, K., and A.K. Srivastava. 1999. DCAMKL1, a brain-specific transmembrane protein on 13q12.3 that is similar to doublecortin (DCX). *Genomics.* 56:121–126. http://dx.doi.org/10.1006/geno.1998.5718

Vasudevan, K.M., D.A. Barbie, M.A. Davies, R. Rabinovsky, C.J. McNear, J.J. Kim, B.T. Hennessy, H. Tseng, P. Pochanard, S.Y. Kim, et al. 2009. AKT-independent signaling downstream of oncogenic PIK3CA mutations in human cancer. *Cancer Cell.* 16:21–32. http://dx.doi.org/10.1016/j.ccr.2009.04.012

Villén, J., and S.P. Gygi. 2008. The SCX/IMAC enrichment approach for global phosphorylation analysis by mass spectrometry. *Nat. Protoc.* 3:1630–1638. http://dx.doi.org/10.1038/nprot.2008.150

Wee, H.J., G. Huang, K. Shigesada, and Y. Ito. 2002. Serine phosphorylation of RUNX2 with novel potential functions as negative regulatory mechanisms. *EMBO Rep.* 3:967–974. http://dx.doi.org/10.1093/embo-reports/kvf193

Zaidi, M. 2007. Skeletal remodeling in health and disease. *Nat. Med.* 13:791–801. http://dx.doi.org/10.1038/nm1593

Zhang, Y., J.A. Ryan, P.E. Di Cesare, J. Liu, C.A. Walsh, and Z. You. 2007. Doublecortin is expressed in articular chondrocytes. *Biochem. Biophys. Res. Commun.* 363:694–700. http://dx.doi.org/10.1016/j.bbrc.2007.09.030

Zhao, M., S.Y. Ko, J.H. Liu, D. Chen, J. Zhang, B. Wang, S.E. Harris, B.O. Oyajobi, and G.R. Mundy. 2009. Inhibition of microtubule assembly in osteoblasts stimulates bone morphogenetic protein 2 expression and bone formation through transcription factor Gli2. *Mol. Cell. Biol.* 29:1291–1305. http://dx.doi.org/10.1128/MCB.01566-08